

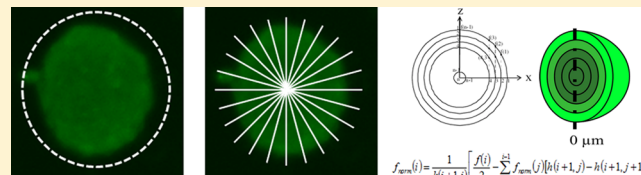
## Multilayer Spheroids To Quantify Drug Uptake and Diffusion in 3D

Toni-Marie Achilli,<sup>†,‡</sup> Stephanie McCalla,<sup>‡,§</sup> Julia Meyer,<sup>†,‡</sup> Anubhav Tripathi,<sup>‡,§</sup> and Jeffrey R. Morgan\*,<sup>†,‡</sup>

<sup>†</sup>Department of Molecular Pharmacology, Physiology and Biotechnology, <sup>‡</sup>Center for Biomedical Engineering, and <sup>§</sup>School of Engineering, Brown University, Providence, Rhode Island 02912, United States

**ABSTRACT:** There is a need for new quantitative *in vitro* models of drug uptake and diffusion to help assess drug toxicity/efficacy as well as new more predictive models for drug discovery. We report a three-dimensional (3D) multilayer spheroid model and a new algorithm to quantitatively study uptake and inward diffusion of fluorescent calcein via gap junction intercellular communication (GJIC). When incubated with calcein-AM, a substrate of the efflux transporter P-glycoprotein (Pgp), spheroids from a variety of cell types accumulated calcein over time. Accumulation decreased in spheroids overexpressing Pgp (HEK-MDR) and was increased in the presence of Pgp inhibitors (verapamil, loperamide, cyclosporin A). Inward diffusion of calcein was negligible in spheroids that lacked GJIC (OVCAR-3, SK-OV-3) and was reduced in the presence of an inhibitor of GJIC (carbenoxolone). In addition to inhibiting Pgp, verapamil and loperamide, but not cyclosporin A, inhibited inward diffusion of calcein, suggesting that they also inhibit GJIC. The dose response curves of verapamil's inhibition of Pgp and GJIC were similar ( $IC_{50}$ : 8  $\mu$ M). The method is amenable to many different cell types and may serve as a quantitative 3D model that more accurately replicates *in vivo* barriers to drug uptake and diffusion.

**KEYWORDS:** ABC transporters, gap junctions, drug transport, drug diffusion



$$f_{\text{sgm}}(i) = \frac{1}{h(i+1,i)} \left[ \frac{f(i)}{2} - \sum_{j=1}^{i-1} f_{\text{sgm}}(j)[h(i+1,j) - h(i+1,j+1)] \right]$$

### INTRODUCTION

A quantitative understanding of drug uptake and diffusion within tissues is an important aspect of successful drug development. At the cellular and multicellular level, diffusion is the primary mechanism for drug movement into cells, avascular tissues, and tumors.<sup>1,2</sup> However, diffusion is tightly controlled by biological barriers including the plasma membrane, transport proteins, vesicular systems, cell adhesion molecules, gap junctions, and cellular efflux pumps.<sup>1–3</sup> The ability to cross these barriers *in vivo* is a key determinant of a drug's absorption, distribution, metabolism, excretion, and toxicity (ADME-Tox) and, ultimately, the success of the drug.<sup>4–7</sup> From the route of administration to the site of action, a drug encounters barriers and transporters before reaching its target. The largest family of transporters is the ATP binding cassette (ABC) transporters, and P-glycoprotein (Pgp) is a member of this family.<sup>7–9</sup> The Pgp transporter is localized to the plasma membrane of cells and is present in both normal and diseased tissues. Normally, Pgp helps to protect sensitive tissues from toxicity by facilitating efflux and preventing the intracellular accumulation of Pgp substrates.<sup>8–15</sup> However, in diseased tissues and the cells of solid tumors, Pgp is sometimes upregulated, increasing resistance to anticancer chemotherapeutics.<sup>10,11</sup> Many drugs of various pharmacological classes are substrates and sometimes inhibitors of this pump.<sup>8,9</sup>

Numerous inhibitors of Pgp have been identified, characterized *in vitro*, and evaluated in the clinic. Although effective *in vitro*, Pgp inhibitors have proven ineffective in the clinic, or have unexpected drug–drug interactions leading to increased toxicity.<sup>16,17</sup> There are three principal *in vitro* methods to

characterize Pgp inhibitors: measurement of the efflux of radiolabeled compounds by a monolayer of cells, measurement of drug-stimulated ATPase activity of Pgp protein, and measurement of calcein-AM uptake by a monolayer of cells.<sup>18–21</sup> Monolayers can measure inhibition of Pgp, but drug uptake and diffusion in these two-dimensional (2D) systems does not accurately replicate the complexity found in a 3D multicell layer environment. The diffusion distance for a drug into a monolayer is relatively short compared to *in vivo* tissues, and biological barriers are not adequately replicated. Current methods to quantify 3D uptake and diffusion in tissues are cumbersome and include the use of microelectrode sensors or radiolabeled molecules, and are not amenable to higher throughput analyses.<sup>21–25</sup>

In this paper, we have developed a new 3D multilayer spheroid model to quantitatively study uptake and diffusion. Using calcein-AM and its fluorescent derivative, calcein, along with wide field fluorescent images, we have calculated the uptake and diffusion of calcein into spheroids of a variety of different cell types. Accumulation of total spheroid calcein was decreased when spheroids overexpressed Pgp and was increased when spheroids were treated with known inhibitors of Pgp

**Special Issue:** Engineered Biomimetic Tissue Platforms for *in Vitro* Drug Evaluation

**Received:** January 2, 2014

**Revised:** March 12, 2014

**Accepted:** March 18, 2014

**Published:** March 18, 2014

(verapamil, loperamide, and cyclosporin A). Inward diffusion of calcein was negligible in spheroids that lacked gap junctional intercellular communication (GJIC) and was reduced when spheroids were treated with a drug (carbenoxolone) known to block GJIC. We also found that two of the Pgp inhibitors (verapamil, loperamide) also inhibited inward diffusion of calcein, suggesting that they are also inhibitors of GJIC.

## ■ EXPERIMENTAL SECTION

### Design, Fabrication, and Casting of Micromolds.

Micromolds used to form hydrogels for forming spheroids were designed using computer design software (SolidWorks Corporation, Concord, MA).<sup>26,27</sup> Designs used for side-view microscopy contained a single row of 21 recesses with rounded bottoms, each recess 400 μm in diameter and 800 μm in depth. Wax molds were produced with a ThermoJet rapid prototyping machine (3D Systems Corporation, Valencia, CA). Polyacrylamide gels were cast from the wax molds. All chemicals were purchased from Sigma Aldrich (St. Louis, MO). A mixture of acrylamide/bis-acrylamide (29:1 ratio), ammonium persulfate (APS), 0.5 M Tris buffer (pH 6.8), and Dulbecco's modified Eagle's medium (DMEM) (Invitrogen, Carlsbad, CA) was degassed. *N,N,N',N'*-Tetramethylethylenediamine was added to initiate polymerization. The solution was pipetted into the wax mold and covered with a coverslip to create a flat bottom on the gel. After 10 min, the hydrogel was removed from the mold, washed several times with DMEM, and incubated overnight in DMEM.

**Cell Culture and Spheroid Formation.** KGN cells, a human granulosa cell line, were grown in DMEM.<sup>28</sup> OVCAR-3 and SK-OV-3 cells were grown in Roswell Park Memorial Institute medium (RPMI; Invitrogen). MCF-7 cells were kindly provided by Dr. Gottesman, NIH Bethesda, MD, and maintained in DMEM.<sup>29</sup> HEK control and HEK transfected cells were obtained from Dr. Robey, NIH Bethesda, MD, and cultured in EMEM.<sup>30</sup> Both media were supplemented with 10% fetal bovine serum (FBS) (Thermo Fisher Scientific, Waltham, MA) and 1% penicillin/streptomycin and grown at 37 °C and 10% CO<sub>2</sub>. Cells were trypsinized using 0.05% trypsin and resuspended to the desired cell concentration. Spheroids that were prestained were formed from cells incubated with 5 μM CellTracker Red CMPTX, CellTracker Green CMFDA, or CellTracker Blue CMAC (Invitrogen) in serum-free DMEM for 1 h prior to trypsinization. 75 μL of the cell suspension was pipetted into the seeding chamber of each gel. Cells were allowed to settle for 20 min, and 4 mL of medium was added. Cells self-assembled for 24 h to form spheroids before experimentation.

**Microscopy.** Horizontal view microscopy was used to measure the height (*z*) of the spheroid from a Mitutouo FS-110 microscope altered to lie on its back. Samples were placed on a translational stage, and brightfield images were taken through the eyepiece using a Nikon Coolpix 900 camera. For standard, *x*-*y* view images, a Carl Zeiss Axio Observer Z1 equipped with an AxioCam MRm camera (Carl Zeiss MicroImaging, Thornwood, NY), an Xcite 120 XL mercury lamp (Exfo Life Sciences Division, Mississauga, Ontario), and an incubation chamber (37 °C, 10% CO<sub>2</sub>) was used to obtain brightfield, phase contrast, and epifluorescent images.

**Image Analysis.** Quantitative image analysis was performed using a custom MATLAB (Mathworks, Natick, MA) program. Briefly, fifty evenly spaced radii were drawn across each spheroid, and fluorescence at each pixel was averaged.

Background fluorescence outside the spheroid was subtracted, taking into account that the fluorescence surrounding the spheroids decreased exponentially and was thus different for different points within the spheroid. Total spheroid fluorescence was determined by the integration of the fluorescent profiles (eq 2). To compare data across experiments, we normalized the spheroids to the fluorescence per depth of single cells at the final time point.

The height (*h*) at each point in the spheroid was calculated using the formula for an ellipse with half-width *a* and half-height *b*, such that

$$h(x) = b \sqrt{1 - \left(\frac{x}{a}\right)^2} \quad (1)$$

The fluorescent intensity at each height was averaged over all spheroids stained with CellTracker dyes [red (*n* = 52), green (*n* = 74), and blue (*n* = 60)]. The total fluorescence at each point is the integrated fluorescence of all cells below it, expressed as

$$F_t(x) = \int_0^{h(x)} C(x, z) \alpha p^2 dz \quad (2)$$

where *C*(*x,z*) is the concentration of the fluorophore along the *y* = 0 plane,  $\alpha$  is the emitted fluorescence per mole of fluorophore, and *p* is the resolution of one pixel (2 μm × 2 μm). The uniformly prestained spheroids have constant fluorophore concentration, *C*<sub>0</sub>. The integral in eq 2 shows that the total fluorescence is linearly related to the height of the spheroid below each point:

$$F_t = C_0 \alpha p^2 h \quad (3)$$

**Uptake of Calcein-AM and Diffusion of Calcein.** To measure uptake and inward diffusion of calcein, medium was removed from the hydrogels containing self-assembled spheroids (24 h) and replaced with serum-free DMEM containing 1 μM calcein-AM (Invitrogen). Fluorescent imaging of calcein began immediately, and images were taken at regular intervals over 135 min at 37 °C and 10% CO<sub>2</sub>. To measure loss of calcein, hydrogels containing spheroids that had been incubated with calcein-AM for 135 min, thus loading the spheroids with calcein, were rinsed with DMEM and incubated in DMEM without calcein-AM. Images were taken once per hour for 11 h, at 37 °C and 10% CO<sub>2</sub>.

**Drug Treatment To Block P-Glycoprotein and Gap Junctions.** Stock solutions of verapamil monohydrochloride hydrate, loperamide hydrochloride, and cyclosporin A (Sigma) (5 μg/mL, 100 μM, and 25 μM, respectively) were used to make working solutions in serum-free DMEM. Hydrogels were equilibrated with a drug-containing medium overnight at 37 °C and 10% CO<sub>2</sub>, and spheroids were self-assembled for 24 h in their respective drug concentration. At these drug concentrations, self-assembly kinetics were unaltered. A working solution of carbenoxolone (CBX) (Sigma) was prepared by diluting appropriate volumes of a 10 mM stock solution into serum-free medium. Spheroids were assembled for 24 h and then pretreated with CBX for 5 h prior to adding calcein-AM for the uptake assay. Medium containing drug and calcein-AM were used for the uptake assay.

**Statistical Analysis.** Two experimental groups were tested for significant variability between sample means using analysis of variance (ANOVA). If significant differences were established, we performed a Bonferroni *t*-test to determine significance.

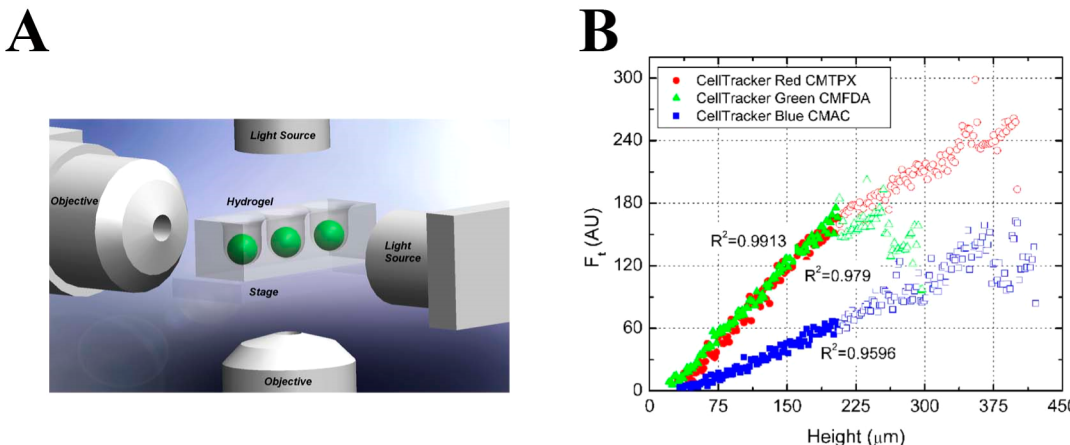


**Figure 1.** Experimental setup to form spheroids and capture wide field fluorescent images. Standard view ( $x, y$ ) and side view ( $z$ ) microscopy were used to obtain fluorescent images of spheroids self-assembled in a micromolded nonadhesive hydrogel (A). Uniformly labeled spheroids of varying sizes were formed from cells stained with CellTracker green, red, or blue dyes, and fluorescent images were taken 24 h after self-assembly. The height ( $z$  dimension) of spheroids of varying sizes that were uniformly labeled red (●), green (▲), or blue (■) was measured and plotted versus peak spheroid fluorescence at the position of maximum fluorescence, maximum cell density (spheroid center) ( $F_t$  (AU)) (B). Up to a critical height of 205  $\mu\text{m}$ , there is a linear relationship between spheroid height and total fluorescence.

## RESULTS

**Determining the Critical Height for Imaging Spheroids.** To quantify the distribution of fluorescent molecules in 3D spheroids using wide field fluorescence, we determined the limits to spheroid size (Figure 1). Prestained (CellTracker dyes) monodispersed cells were seeded onto a micromolded nonadhesive hydrogel, whereon they self-assembled spheroids after 24 h. Using side view and conventional view microscopy, we obtained fluorescent images and  $x, y, z$  measurements of a size range of spheroids. Peak fluorescence intensity at the center or thickest location of the spheroid showed a linear relationship between spheroid height and fluorescence for all three fluorophores up to a critical spheroid height of 205  $\mu\text{m}$ , implying that 100% of the emitted fluorescent light (red, blue, green) was captured. Subsequent studies used spheroids below this critical height. We also used a MATLAB algorithm to generate an average 2D radial profile of fluorescence intensity from fifty radial lines, and this average radial profile was parabolic, consistent with the predicted theoretical profile (eq 1).

**Uptake and Diffusion by Multilayer Spheroids.** To measure uptake and diffusion, spheroids were incubated with calcein-AM (1  $\mu\text{M}$ ) and images of fluorescent calcein were taken every fifteen minutes for 135 min (Figure 2). Calcein fluorescence in the entire spheroid increased rapidly over time and started to plateau after about 60 min. We used our MATLAB algorithm to generate an average 2D radial profile of fluorescence at each time point, and this time series also showed that total calcein fluorescence increased throughout the 135 min (area under curve). However, none of the 2D radial profiles attained the full parabolic curve seen with uniformly stained spheroids. Maximum calcein fluorescence was not in the center of the spheroid (point of greatest cell number), rather, it was located near the outer edge of the spheroid. This indicated that as uptake and inward diffusion occurred over time, the highest concentration of calcein was in the outer layer of the spheroid and calcein concentration decreased toward the spheroid core.

To deconvolve this fluorescent signal into an average 3D radial profile, the spheroid was estimated as a series of

concentric spheres (multilayers). Each layer (shell) was 14  $\mu\text{m}$  in width and contained a homogeneous concentration of fluorescent calcein (Figure 2). The total fluorescence  $f(i)$  at the  $X_i$  layer is the sum of the fluorescence contribution from all shells at  $X_i$ . Mathematically, we can write the total fluorescence as

$$f(i) = 2 \sum_{j=1}^i f_{\text{norm}}(j)[h(i+1, j) - h(i+1, j+1)] \quad (4)$$

Here,  $f_{\text{norm}}(j)$  is the fluorescence/height in the  $i$ th shell and  $h(i, j)$  is the height at point  $(X_i, Y_j)$ . Note  $h(i, i) = 0$  lies at the centerline of the spheroid. Hence, we determined  $f_{\text{norm}}(j)$  by sequentially subtracting the fluorescence due to inner shells from the total fluorescence  $f(i)$  at  $X_i$ . Equation 4 results in the following iterative formula:

$$f_{\text{norm}}(i) = \frac{1}{h(i+1, i)} \left[ \frac{f(i)}{2} - \sum_{j=1}^{i-1} f_{\text{norm}}(j)[h(i+1, j) - h(i+1, j+1)] \right] \quad (5)$$

This analysis was used to plot calcein concentration as a function of 3D radius. The core was taken as  $\geq 14 \mu\text{m}$  from the center in the smallest dimension to ensure the core contained whole cells. Even at later time points, the concentration of calcein in the core did not reach the same concentration as the outer shell, indicative of cellular barriers to diffusion. As calcein-AM is taken up by the cells of the outer spheroid layer, some is pumped out by the action of Pgp and some is converted to fluorescent calcein by intercellular esterases. This intercellular calcein diffuses to the inner layers of the spheroid via GJIC. It is important to note that calcein-AM surrounds the spheroid and this spheroid ( $r = 100 \mu\text{m}$ ) occupies a volume of  $4 \times 10^6 \mu\text{m}^3$ . In the absence of a spheroid and the barriers it creates, calcein-AM and calcein would complete their diffusion into this volume of medium (diffusivity = 260 and 500  $\mu\text{m}^2/\text{s}$ , respectively) within  $\sim t = r^2/D \sim 10\text{--}20 \text{ s}$ . Thus, the spheroid is a complex barrier to calcein-AM and calcein diffusion.

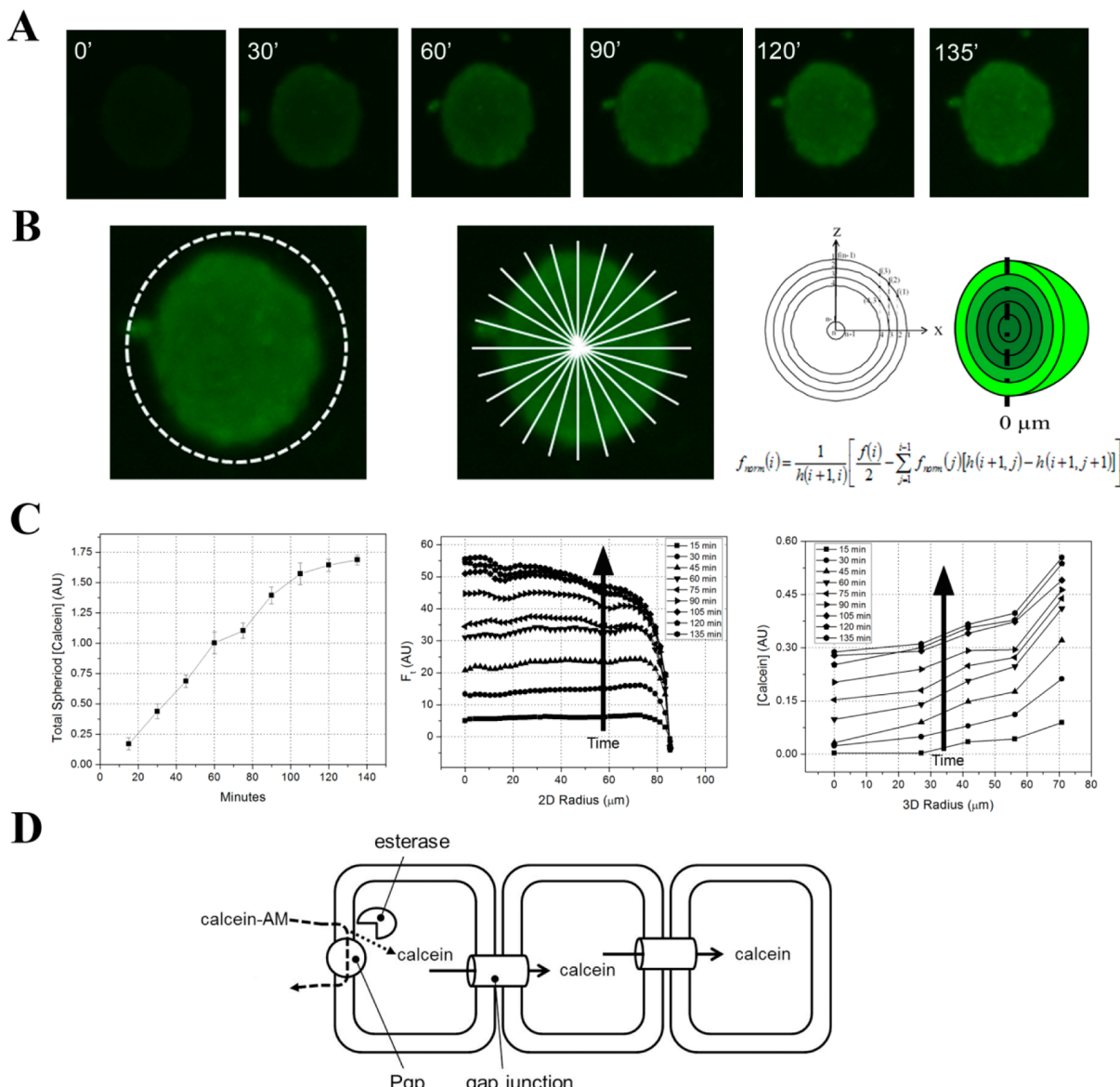


**Figure 2.** Quantification of uptake and diffusion of fluorescent calcein in multicellular spheroids. Spheroids of KGN cells were incubated with  $1 \mu\text{M}$  calcein-AM and time-lapse fluorescent images taken over 135 min (A). The total spheroid calcein, the 2D radial distribution of calcein, and the 3D radial distribution of calcein were calculated from the images (B, C). Schematic showing multiple cell layers of a spheroid connected by GJIC (D). Calcein-AM surrounding the spheroid is actively effluxed by Pgp, but some gains access to the cytoplasm where it is converted by esterases into fluorescent calcein that is trapped within the cell. Calcein can diffuse inward toward the spheroid core via GJIC connecting multiple cell layers.

To measure uptake and diffusion in spheroids of other cell types, we formed spheroids from HEK, MCF-7, OVCAR-3, and KGN cells, incubated them with calcein-AM, and measured calcein over time from fluorescent images (Figure 3). From this time series, we computed total calcein fluorescence in the entire spheroid and the 2D and 3D radial profiles of calcein fluorescence. For all spheroids, total calcein accumulated rapidly over time and started to plateau after about 40–60 min. However, the 2D and 3D radial profiles of calcein fluorescence were significantly different depending on cell type. KGN, MCF-7, and HEK spheroids showed the greatest diffusion of calcein into the core, whereas OVCAR-3 spheroids showed little if any calcein fluorescence in the core with most of the calcein confined to the outer layer. Spheroids made with SK-OV-3 cells, another ovarian cancer cell line that lacks GJIC,

had profiles similar to OVCAR-3 cells with little diffusion of calcein into the spheroid core (data not shown).<sup>31</sup>

To determine the effects of efflux pump overexpression, we performed the calcein assay with HEK-MDR cells transfected with Pgp, an efflux pump known to transport calcein-AM (Figure 4). The rate of increase in total spheroid calcein fluorescence was significantly lower in spheroids of HEK-MDR cells versus parental HEK spheroids. In the presence of verapamil, an inhibitor of Pgp, total spheroid calcein fluorescence increased in untransfected cells which have some endogenous Pgp expression and increased significantly in HEK-MDR cells.

**Multilayer Uptake and Diffusion in the Presence of Pgp and GJIC Inhibitors.** To determine the effects of verapamil on the diffusion of calcein, we measured the radial distribution of calcein (Figure 5). A time series of 2D radial

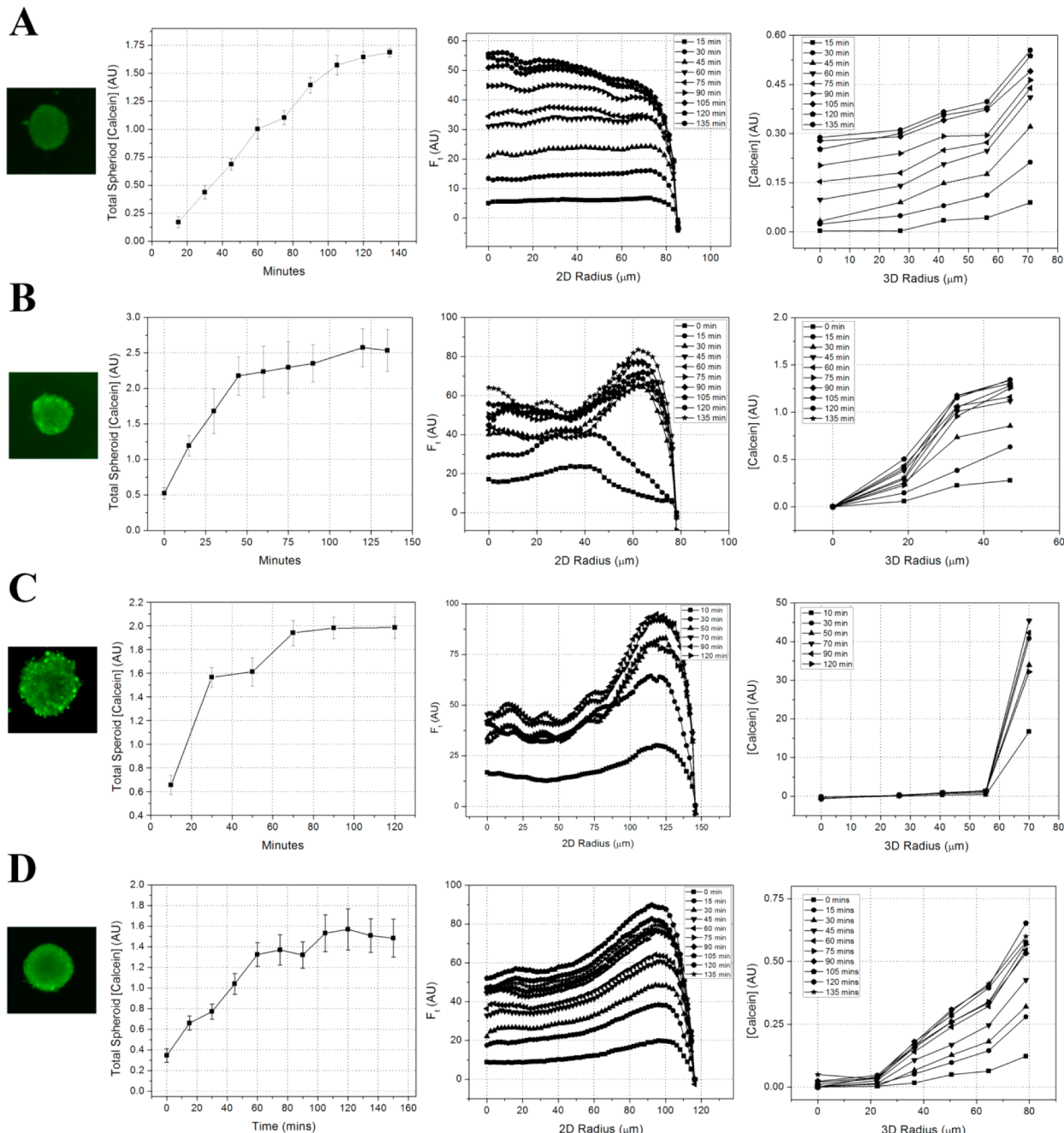


**Figure 3.** Uptake and diffusion of fluorescent calcein in multicellular spheroids. Spheroids of KGN (A), MCF-7 (B), OVCAR-3 (C), and HEK (D) cells were incubated with 1  $\mu$ M calcein-AM and time-lapse fluorescent images taken over 135 min. Total calcein fluorescence in the entire spheroid was quantified over time ( $n = 15\text{--}26$ ). Regardless of cell type used to form the spheroids, total spheroid calcein accumulated rapidly over time and started to plateau after about 40–60 min. The 2D radial distribution of calcein within these spheroids at each time point was quantified, and the resulting 3D radial distribution of calcein within these spheroids at each time point was also calculated. The 2D and 3D radial profiles were significantly different depending on cell type. KGN, MCF-7, and HEK spheroids showed the greatest diffusion of calcein into the core, whereas OVCAR-3 spheroids lacking GJIC showed little if any diffusion of calcein into the core with most of the calcein confined to the outer layer of cells.

profiles showed that total spheroid fluorescence increased with verapamil treatment, consistent with inhibition of Pgp. However, the shape of the 2D radial profiles of verapamil-treated samples was different from that of untreated controls. Fluorescence of the outer layer versus the core was increased, indicating more calcein in the outer layer of the drug-treated samples. Our 3D analysis showed that, in addition to increasing the total calcein in a spheroid, verapamil treatment altered the concentration gradient within the spheroid. Calcein concentration was increased in the outer layer, as would be expected

by inhibition of the Pgp, but calcein concentration was not elevated in the core as a result of the increased levels in the outer layer. High levels of calcein in the outer layer should lead to increased levels in the core, but surprisingly, our 3D analysis showed that calcein levels in the core were higher in untreated samples than in those treated with verapamil.

To determine if other inhibitors of Pgp had similar effects, we tested loperamide and cyclosporin A (Table 1). Total calcein in spheroids treated with loperamide (5  $\mu$ M), cyclosporin A (25  $\mu$ M), and verapamil (25  $\mu$ M) was

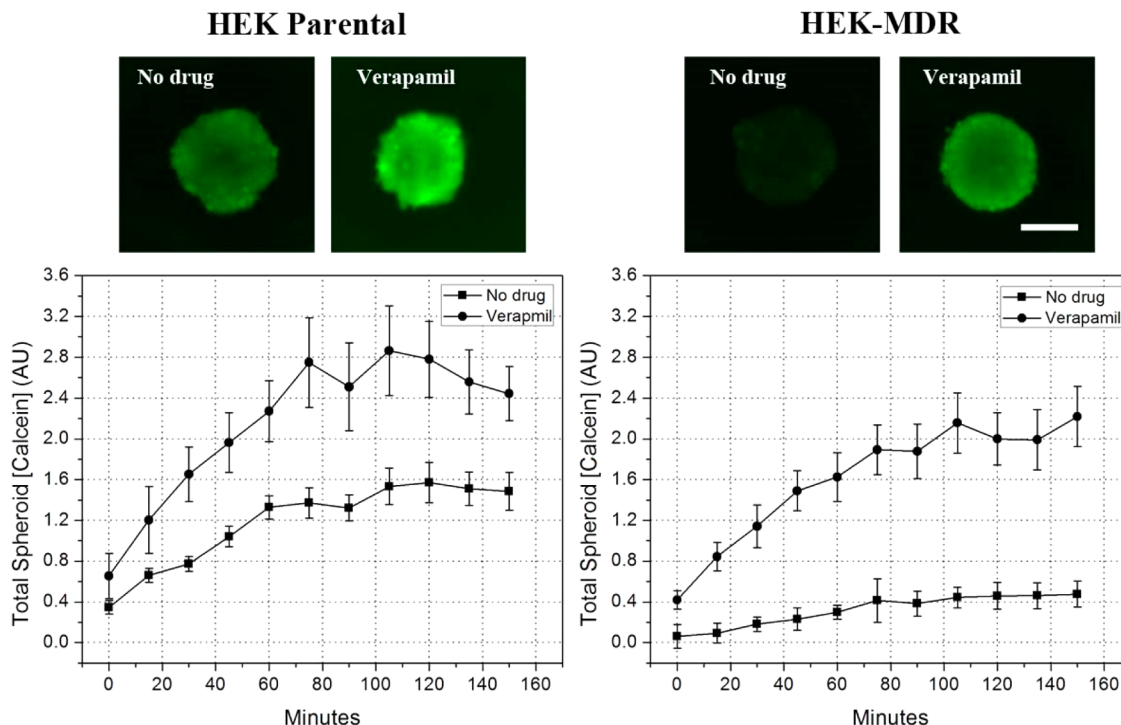


**Figure 4.** Efflux pump overexpression inhibits calcein uptake. Spheroids of HEK cells or HEK-MDR cells transfected to overexpress Pgp were incubated with 1  $\mu$ M calcein-AM and time-lapse fluorescent images taken over 135 min. Images at 135 min. Scale bar 100  $\mu$ m. Total calcein fluorescence in the entire spheroid was quantified over time ( $n = 18$ ). The rate of increase in total spheroid calcein was significantly lower in spheroids of HEK-MDR cells versus HEK spheroids. In the presence of verapamil (25  $\mu$ M), an inhibitor of Pgp, total spheroid calcein fluorescence increased in untransfected cells that have some endogenous Pgp and increased significantly in HEK-MDR cells overexpressing Pgp.

significantly increased compared to untreated controls, consistent with their activities as inhibitors of Pgp. Further, compared to untreated controls, levels of calcein were significantly increased in the outer shell of all drug treated spheroids.

To determine if inward diffusion of calcein was altered by any of the Pgp inhibitors, we used our 3D analysis to determine what fraction (%) of the total calcein was located in the outer shell versus the inner core. In verapamil and loperamide treated samples, the percentage of calcein in the outer shell was increased compared to control, while the percentage of calcein in the core was decreased. After treatment with cyclosporin A, calcein concentration increased in all compartments, such that the percentage of calcein in the shell and core compartments was not significantly different from that in their respective compartments in untreated samples. This indicates that cyclosporin A did not alter inward diffusion of calcein.

Since diffusion of calcein requires GJIC, we tested the effects of CBX (CBX), an inhibitor of gap junctions.<sup>32</sup> As expected, CBX treatment decreased inward diffusion of calcein. After 135 min of uptake, only  $0.5 \pm 2\%$  of the total calcein was located in the core of spheroids treated with CBX (100  $\mu$ M) versus  $15 \pm 3\%$  in untreated spheroids ( $n = 18$ ). Likewise, the fraction of calcein in the outer shell of CBX treated spheroids was increased versus untreated controls ( $52 \pm 4\%$  versus  $27 \pm 3\%$ ). In addition to altering inward diffusion of calcein, surprisingly, we found that CBX treatment increased the total amount of calcein fluorescence in the entire spheroid. After 135 min, total calcein in CBX treated spheroids was increased  $2.3 \pm 0.4$  fold versus untreated spheroids, suggesting that, in addition to being an inhibitor of GJIC, CBX also inhibits Pgp.

Since verapamil and CBX inhibited both Pgp and GJIC, we did a dose response to compare their potencies (Figure 6). Spheroids were incubated with calcein-AM in the presence of varying doses of verapamil or CBX and fluorescent images obtained after 75 min. The 3D radial profiles revealed that increasing concentrations of verapamil and CBX both resulted in increased calcein uptake (area under curve), but that calcein was more localized to the outer shell with CBX treatment (shape of curve). To determine the dose response with respect to inhibition of Pgp, we plotted total spheroid calcein ( $n = 15$ ) as a function of drug concentration. For verapamil, half-maximal response was 8.5  $\mu$ M, whereas for CBX, half-maximal response was 81  $\mu$ M. There was a linear dose response for CBX versus verapamil which rose rapidly and reached a plateau.

We used the same data to determine the dose response with respect to inhibition of GJIC by calculating a drug's ability to increase the fraction of calcein compartmentalized to the outer shell. For verapamil, half-maximal response with respect to GJIC inhibition was 8.6  $\mu$ M, similar to the concentration that elicited half-maximal inhibition of Pgp. For CBX, half-maximal response for GJIC inhibition was 9.4  $\mu$ M, significantly lower than the concentration that elicited half-maximal inhibition of Pgp.

To rule out the possibility that verapamil's inhibition of GJIC might be mediated by verapamil's calcium channel-blocking activity and mediated via a change in intracellular calcium, we tested nitrendipine, a highly specific calcium channel blocker. Nitrendipine had no effect on calcein compartmentalization (data not shown).

To determine if CBX might be increasing total spheroid calcein by slowing the loss of calcein rather than by inhibiting Pgp, we measured the kinetics of calcein loss (Figure 7).

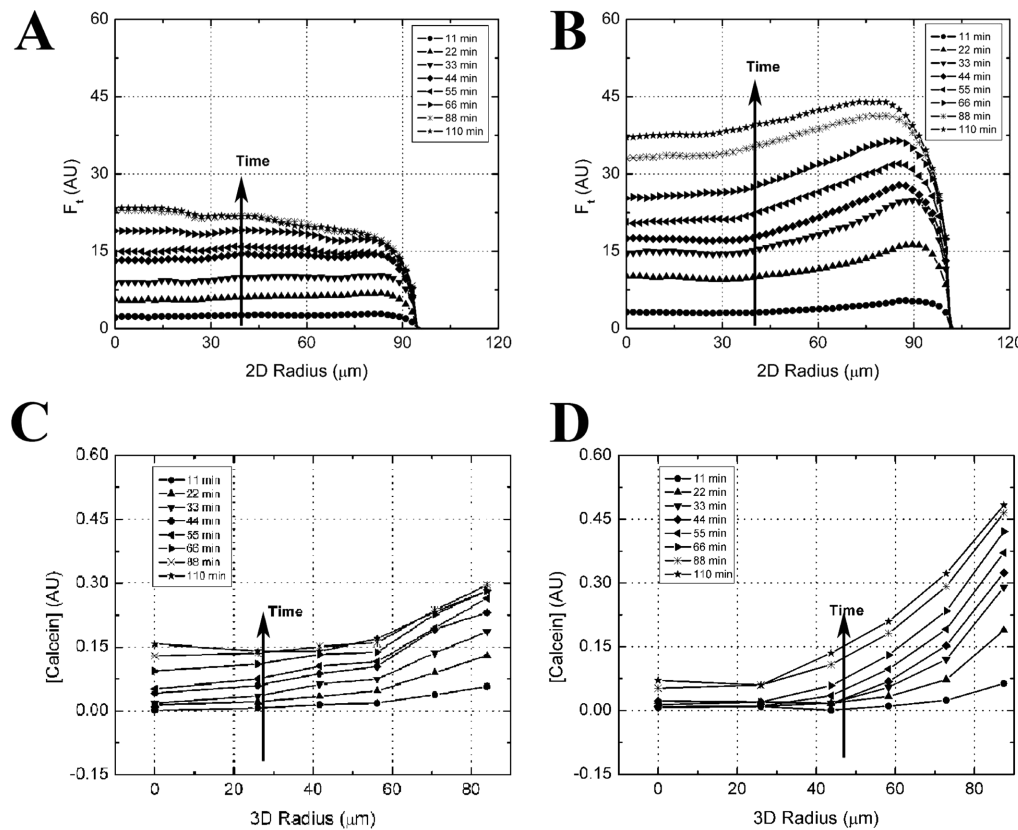


**Figure 5.** Verapamil increases total spheroid calcein, but decreases diffusion of calcein. KGN spheroids were incubated with 1  $\mu\text{M}$  calcein-AM in the presence of verapamil (untreated, A, C; 25  $\mu\text{M}$ , B, D), and images were taken every 11 min for 110 min. A time series of 2D radial profiles (A, B) shows that total fluorescence of all spheroids ( $F_t$  (AU)) increases with time. Verapamil treatment increases total spheroid fluorescence over untreated controls, but fluorescence is preferentially located in the outermost layer of cells. The quantitative 3D radial profiles of calcein concentration ([Calcein] (AU)) (C, D) reveal that although verapamil increases uptake in the outer layer over control (every time point), calcein concentration at the center of the spheroid does not increase.

**Table 1**

	control		verapamil		loperamide		cyclosporin A		
	[calcein]	%	[calcein]	%	[calcein]	%	[calcein]	%	
	outer shell	0.40 $\pm$ 0.05	26 $\pm$ 2	1.12 $\pm$ 0.14*	37 $\pm$ 4*	0.98 $\pm$ 0.16*	40 $\pm$ 4*	1.33 $\pm$ 0.21*	32 $\pm$ 5
	inner core	0.19 $\pm$ 0.05	13 $\pm$ 2	0.11 $\pm$ 0.03*	3 $\pm$ 1*	0.1 $\pm$ 0.4*	4 $\pm$ 2*	0.72 $\pm$ 0.16*	17 $\pm$ 4
	total	1.72 $\pm$ 0.09		3.13 $\pm$ 0.23*		2.41 $\pm$ 0.18*		3.22 $\pm$ 0.19*	

Spheroids with and without CBX treatment were incubated with calcein-AM for 135 min. Medium with calcein-AM was then removed and replaced with fresh medium, and fluorescent images were taken for 20 h to quantify the rate of calcein loss. Calcein fluorescence decreased at the same initial rate for control and CBX treated spheroids with half-lives of 5.3 and 5.9 h respectively.

## DISCUSSION

Drug uptake, transport, diffusion, and elimination from tissues are important properties governing the efficacy and potential toxicity of drugs and drug candidates. Efflux transporters, such as Pgp, are well-known regulators of drug bioavailability, and their modulation, either intentionally via inhibitors or unintentionally via the side effects of certain drugs, can have profound pharmacological effects.<sup>4–7</sup> Some efflux transporters can be upregulated by solid tumors causing multidrug resistance, so there is an active interest to identify more effective inhibitors

for use in chemotherapy.<sup>10,11</sup> Thus, there is a need for new *in vitro* models to predict drug toxicity and unwanted drug–drug interactions and a need for models to discover new and more effective inhibitors of efflux transporters associated with multidrug resistance. Although monolayers of cells have been useful for defining some of these transport parameters and have been used to identify inhibitors of efflux pumps, such as Pgp,<sup>11,18,21</sup> there is growing recognition that 2D cell culture may not adequately replicate the biological complexities of the 3D *in vivo* environment.

3D models have been used to investigate transport properties, molecular gradients, and cellular gradients, but often these methods require complex experimental and analytical procedures such as two-photon microscopy,<sup>33</sup> radiolabeled probes,<sup>23</sup> tissue sectioning,<sup>24</sup> or mathematical models.<sup>34</sup> The method described here readily lends itself to quantitative uptake and diffusion studies. Spheroids are uniform in size, and spheroid geometry is well-defined because, in

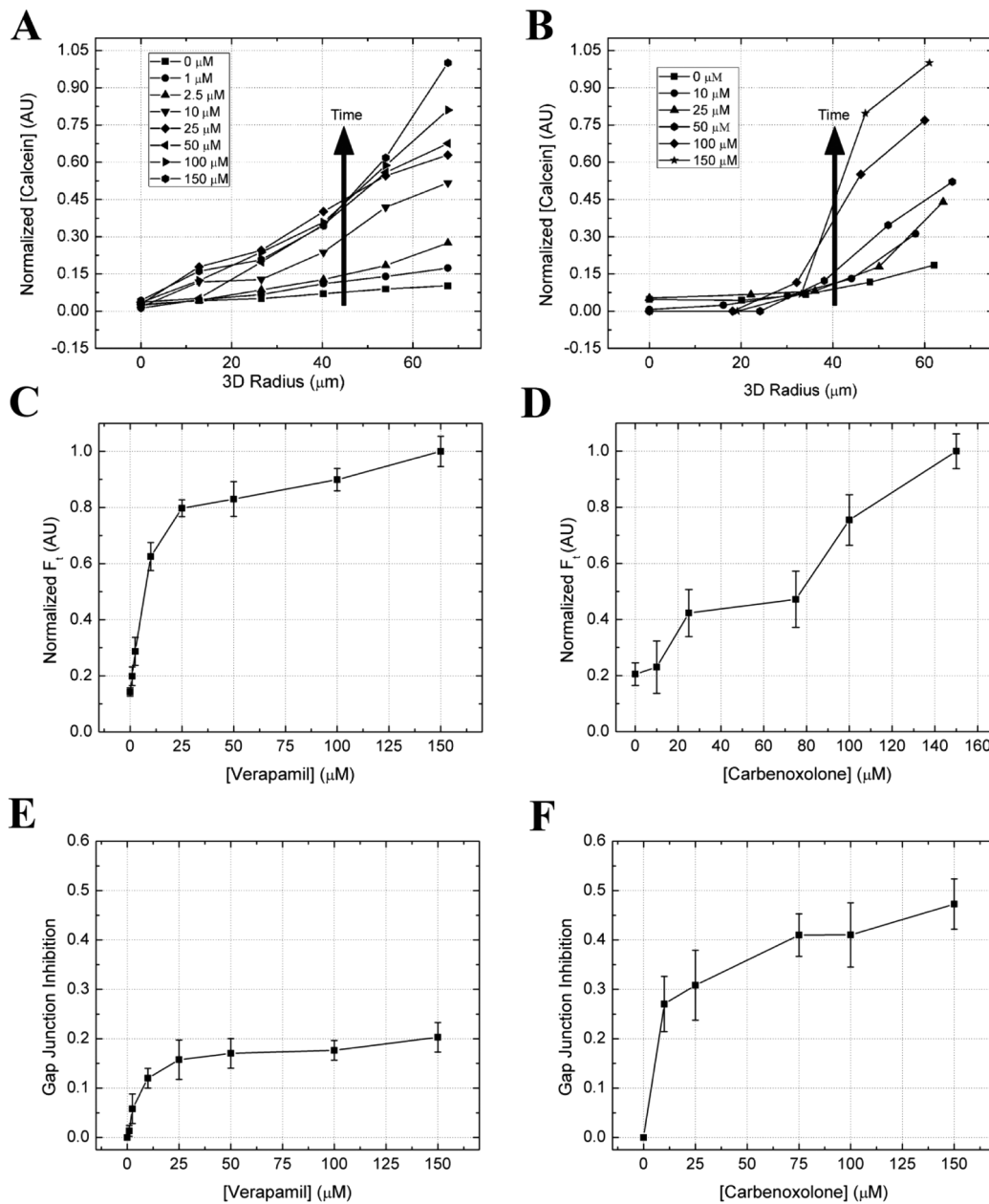


**Figure 6.** Dose responses of verapamil and CBX inhibition of Pgp and GJIC. KGN spheroids were incubated with 1  $\mu$ M calcein-AM in the presence of varying doses of verapamil (A, C, E) or CBX (B, D, F) and fluorescent images obtained after 75 min. The 3D radial profiles of drug treated spheroids (A, B) revealed that increasing concentrations of verapamil and CBX both resulted in increased calcein uptake, but that calcein was more localized to the outer shell with CBX treatment. To determine dose response with respect to inhibition of Pgp (C, D) total calcein uptake by spheroids ( $n = 15$ ) as a function of drug concentration is plotted. To aid comparison, data is normalized to the highest point. For verapamil, half-maximal response was 8.5  $\mu$ M, whereas for CBX, half-maximal response was 81  $\mu$ M. To determine the dose response for GJIC inhibition (E, F), the drug's ability to increase the fraction of calcein compartmentalized to the outer shell was calculated. If the fraction of calcein was the same as that in the untreated control, this was zero percent inhibition. If all calcein was confined to the outer shell, this was 100% inhibition. For verapamil, half-maximal response was 8.6  $\mu$ M, similar to the concentration that elicited half-maximal inhibition of Pgp. For CBX, half-maximal response for inhibition of GJIC was 9.4  $\mu$ M, significantly lower than the concentration that elicited half-maximal inhibition of Pgp. When comparing the maximal responses, CBX inhibited GJIC to a greater extent than verapamil.

addition to measurements of the  $x$ ,  $y$  dimensions, the  $z$  dimension is measured. Spheroids are surrounded by cell culture medium; thus uptake occurs uniformly around the entire surface area. Spheroids are all formed on the same optical plane, making it easy to obtain a time series of fluorescent images from which data on kinetics can be obtained. Precise measurements of a spheroid's geometry and its radial symmetry allowed us to develop an algorithm to calculate the radial

distribution of a fluorescent molecule from wide field fluorescent images.

In this paper, we've used this model to quantify both the uptake and diffusion of fluorescent calcein. Calcein-AM, the nonfluorescent precursor of calcein, is a substrate of the Pgp efflux pump, and fluorescent calcein diffuses into the spheroid via GJIC connecting cell layers.<sup>35</sup> We measured total calcein fluorescence in the entire spheroid, and we measured the

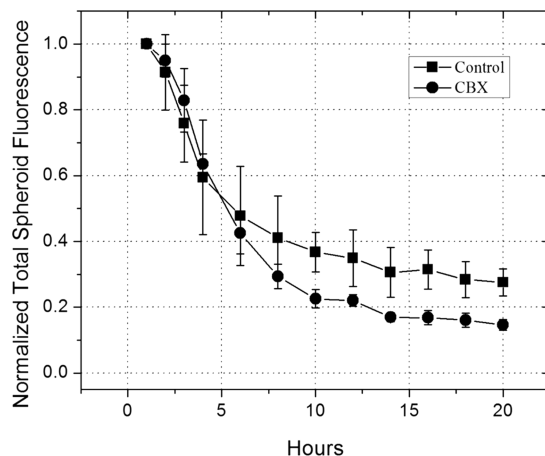


**Figure 7.** CBX does not increase total spheroid calcein by slowing calcein loss. KGN spheroids with and without CBX treatment were incubated with 1  $\mu$ M calcein-AM for 135 min. Calcein-AM was then removed and replaced with drug-free medium. Images were taken once per hour for 20 h to determine the rate of calcein loss, and data was normalized to the initial fluorescence. Loss from the entire spheroid was measured by the total spheroid fluorescence and decreased at the same initial rate for control and CBX treated spheroids.

diffusion of calcein into the spheroid. Spheroids formed from a variety of cell lines all accumulated fluorescent calcein with time, but they differed with regard to their rate of calcein accumulation. When compared to untransfected control HEK spheroids, the rate of calcein accumulation was low in transfected HEK-MDR spheroids overexpressing Pgp. This reduced rate could be reversed by the addition of verapamil, an inhibitor of Pgp. Likewise, when other inhibitors of Pgp were tested (loperamide and cyclosporin A), the rate of accumulation of total spheroid calcein was increased. Although all spheroids accumulated calcein, they differed with regard to how much calcein diffused into the core of the spheroid. Calcein failed to diffuse into spheroids of cells that lack GJIC such as OVCAR-3 and SK-OV-3.<sup>31</sup> Likewise, when spheroids were treated with CBX, a well-known inhibitor of GJIC,<sup>32,33</sup> calcein diffusion was also inhibited.

By quantifying both total spheroid calcein and the diffusion of calcein into the spheroid, we observed previously uncharacterized activities of some of the drugs we tested. For example, verapamil, loperamide, and cyclosporin A are all well-known inhibitors of Pgp, and all three increased total calcein in the spheroid. However, quantification of calcein diffusion into the spheroid showed that verapamil and loperamide inhibited diffusion, whereas cyclosporin A did not: calcein diffusion was the same as in untreated controls. These results suggest that verapamil and loperamide also inhibit GJIC, an activity and novel finding not previously reported for these drugs.

Another unexpected activity that was found because we quantified both total spheroid calcein and calcein diffusion was CBX's inhibition of Pgp. As expected, CBX inhibited calcein diffusion by blocking GJIC; however, CBX also increased total spheroid calcein, consistent with inhibiting Pgp. We ruled out the possibility that CBX mediated its effects by decreasing the loss of total spheroid calcein. When we used both assays to compare the dose responses of verapamil and CBX, we found that while both drugs inhibited Pgp and GJIC, verapamil was more potent at inhibiting Pgp, whereas CBX was more potent and more effective at inhibiting GJIC. Verapamil is a

competitive inhibitor of Pgp,<sup>8,9</sup> and interestingly, the dose response curves of verapamil's inhibition of Pgp and GJIC were very similar. The same dose (8  $\mu$ M) elicited half-maximal response for both activities. All transporters on KGN spheroids have not been fully characterized, nor have we determined if Pgp expression is in any way polarized in KGN spheroids. In addition to Pgp, calcein-AM is a substrate for MRPs/Mrps and calcein is a substrate for MRP. Endogenous levels of these other transporters could affect the level and distribution of calcein in the KGN spheroids as well as the response to various inhibitors. Doses of inhibitors were chosen with Pgp in mind. To help rule out the possibility that diffusion of Pgp inhibitors into the spheroids might be limiting, we exposed our monodispersed cells continuously to verapamil, loperamide, and cyclosporin A while they were self-assembling spheroids and when the spheroids were tested for uptake. We were unable to expose monodispersed cells to CBX because, as we have shown previously, CBX's action on connexons disrupts self-assembly.<sup>36</sup>

Verapamil, loperamide, and cyclosporin A are well-known inhibitors of Pgp, but they are used clinically for other purposes at significantly lower doses. Verapamil blocks voltage-dependent calcium channels and is used to treat hypertension.<sup>37</sup> When tested for the treatment of multidrug resistance, low doses were ineffective and high doses caused cardiotoxicity.<sup>17,38,39</sup> Interestingly, the KGN cells we tested express connexon 43, the same connexon expressed by cardiomyocytes.<sup>40</sup> Loperamide is an opioid-receptor agonist whose primary use is the treatment of diarrhea, but it can also affect calcium levels and is a substrate for and an inhibitor of Pgp.<sup>18</sup> Cyclosporin A, an immunosuppressant used to prevent graft rejection, had the most success with multidrug resistance of retinoblastoma.<sup>41,42</sup> However, its immunosuppressant activity precluded further use and its nonimmunosuppressant derivative has had little success in the clinic.<sup>43</sup>

The 3D model described here can easily be extended to other cell types. We and others have shown that numerous cell types including primary human cells will self-assemble 3D spheroids including cardiomyocytes in this system.<sup>44</sup> Moreover, mixtures of two different cell types often self-sort during self-assembly with one cell type forming the inner core and the other cell type forming the outer coating of the spheroid. These layered spheroids may be useful for replicating heterotypic cell interactions seen in more physiologic barriers to drug uptake. Lastly, 3D models may be useful for discovering new more effective inhibitors of efflux transporters responsible for multidrug resistance and helpful in the early identification of possible side effects and drug–drug interactions of drug candidates.

## CONCLUSION

Multicellular spheroids more accurately replicate *in vivo* barriers to drug uptake and diffusion than 2D monolayers of cells. The quantitative model described here measures uptake and diffusion of calcein through multiple cell layers of a 3D spheroid and assesses the activities of both Pgp and GJIC with respect to efflux of calcein-AM and diffusion of calcein. The model has uncovered previously unknown effects of some drugs, is amenable to many different cell types, and may be useful for the assessment of drug toxicity as well as a model for drug discovery.

## AUTHOR INFORMATION

### Corresponding Author

\*Brown University, G-B 393, Biomed Center 171 Meeting St., Providence, RI 02912. Tel: (401) 863-9879. Fax: (401) 863-1753. E-mail: Jeffrey\_Morgan@Brown.edu.

### Notes

The authors declare the following competing financial interest(s): J.R.M has an equity interest in Microtissues, Inc. This relationship has been reviewed and managed by Brown University in accordance with its conflict of interest policies.

## ACKNOWLEDGMENTS

This work was funded in part by the National Institutes of Health (R01EB008664-01A1) and seed funds from the Johnson & Johnson Corporate Office of Science & Technology and the Brown Technology Ventures Office. Authors would also like to thankfully acknowledge partial support from National Aeronautics and Space Agency (NASA) and the generous support of Donna McGraw Weiss '89 and Jason Weiss.

## ABBREVIATIONS USED

ABC, ATP binding cassette; ADME-Tox, absorption, distribution, metabolism, excretion, and toxicity; CBX, carbenoxolone; DMEM, Dulbecco's modified Eagle's medium; FBS, fetal bovine serum; GJIC, gap junctional intercellular communication; Pgp, P-glycoprotein; RPMI, Roswell Park Memorial Institute medium

## REFERENCES

- (1) Jang, S. H.; Wientjes, M. G.; Lu, D.; Au, J. L. Drug delivery and transport to solid tumors. *Pharm. Res.* **2003**, *20*, 1337–1350.
- (2) Minchinton, A. I.; Tannock, I. F. Drug penetration in solid tumours. *Nat. Rev. Cancer* **2006**, *6*, 583–592.
- (3) Elliott, N. T.; Yuan, F. A review of three-dimensional in vitro tissue models for drug discovery and transport studies. *J. Pharm. Sci.* **2011**, *100*, 59–74.
- (4) Szakacs, G.; Varadi, A.; Ozvegy-Laczka, C.; Sarkadi, B. The role of ABC transporters in drug absorption, distribution, metabolism, excretion and toxicity (ADME-Tox). *Drug Discovery Today* **2008**, *13*, 379–393.
- (5) Shugarts, S.; Benet, L. Z. The role of transporters in the pharmacokinetics of orally administered drugs. *Pharm. Res.* **2009**, *26*, 2039–2054.
- (6) Varma, M. V.; Ashokraj, Y.; Dey, C. S.; Panchagnula, R. P-glycoprotein inhibitors and their screening: a perspective from bioavailability enhancement. *Pharmacol. Res.* **2003**, *48*, 347–359.
- (7) Giacomini, K. M.; et al. Membrane transporters in drug development. *Nat. Rev. Drug Discovery* **2010**, *9*, 215–236.
- (8) Borst, P.; Oude Elferink, R. Mammalian ABC transporters in health and disease. *Annu. Rev. Biochem.* **2002**, *71*, 537–592.
- (9) Ambudkar, S. V.; et al. Biochemical, cellular, and pharmacological aspects of the multidrug transporter. *Annu. Rev. Pharmacol. Toxicol.* **1999**, *39*, 361–398.
- (10) Fojo, A. T.; et al. Expression of a multidrug-resistance gene in human tumors and tissues. *Proc. Natl. Acad. Sci. U.S.A.* **1987**, *84*, 265–269.
- (11) Szakacs, G.; Paterson, J. K.; Ludwig, J. A.; Booth-Genthe, C.; Gottesman, M. M. Targeting multidrug resistance in cancer. *Nat. Rev. Drug Discovery* **2006**, *5*, 219–234.
- (12) Cecchelli, R.; et al. Modelling of the blood-brain barrier in drug discovery and development. *Nat. Rev. Drug Discovery* **2007**, *6*, 650–661.
- (13) Fellner, S.; et al. Transport of paclitaxel (Taxol) across the blood-brain barrier in vitro and in vivo. *J. Clin. Invest.* **2002**, *110*, 1309–1318.
- (14) Fromm, M. F. Importance of P-glycoprotein at blood-tissue barriers. *Trends Pharmacol. Sci.* **2004**, *25*, 423–429.
- (15) Letrent, S. P.; et al. P-glycoprotein-mediated transport of morphine in brain capillary endothelial cells. *Biochem. Pharmacol.* **1999**, *58*, 951–957.
- (16) Sikic, B. I.; et al. Modulation and prevention of multidrug resistance by inhibitors of P-glycoprotein. *Cancer Chemother. Pharmacol.* **1997**, *40* (Suppl.), S13–S19.
- (17) Aszalos, A. Drug-drug interactions affected by the transporter protein, P-glycoprotein (ABCB1, MDR1) II. Clinical aspects. *Drug Discovery Today* **2007**, *12*, 838–843.
- (18) Polli, J. W.; et al. Rational use of in vitro P-glycoprotein assays in drug discovery. *J. Pharmacol. Exp. Ther.* **2001**, *299*, 620–628.
- (19) Rautio, J.; et al. In vitro p-glycoprotein inhibition assays for assessment of clinical drug interaction potential of new drug candidates: a recommendation for probe substrates. *Drug Metab. Dispos.* **2006**, *34*, 786–792.
- (20) Keogh, J. P.; Kunta, J. R. Development, validation and utility of an in vitro technique for assessment of potential clinical drug-drug interactions involving P-glycoprotein. *Eur. J. Pharm. Sci.* **2006**, *27*, 543–554.
- (21) Szeremey, P.; et al. Comparison of 3 assay systems using a common probe substrate, calcein AM, for studying P-gp using a selected set of compounds. *J. Biomol. Screening* **2011**, *16*, 112–119.
- (22) Nederman, T. Effects of vinblastine and 5-fluorouracil on human glioma and thyroid cancer cell monolayers and spheroids. *Cancer Res.* **1984**, *44*, 254–258.
- (23) Nederman, T.; Carlsson, J. Penetration and binding of vinblastine and 5-fluorouracil in cellular spheroids. *Cancer Chemother. Pharmacol.* **1984**, *13*, 131–135.
- (24) Risberg, B.; Grontoft, O.; Westholm, B. Origin of carcinoma in secretory endometrium—a study using a whole-organ sectioning technique. *Gynecol. Oncol.* **1983**, *15*, 32–41.
- (25) Hwang, C. W.; Wu, D.; Edelman, E. R. Physiological transport forces govern drug distribution for stent-based delivery. *Circulation* **2001**, *104*, 600–605.
- (26) Youssef, J.; Nurse, A. K.; Freund, L. B.; Morgan, J. R. Quantification of the forces driving self-assembly of three-dimensional microtissues. *Proc. Natl. Acad. Sci. U.S.A.* **2011**, *108*, 6993–6998.
- (27) Napolitano, A. P.; Chai, P.; Dean, D. M.; Morgan, J. R. Dynamics of the Self-Assembly of Complex Cellular Aggregates on Micro-Molded Non-Adhesive Hydrogels. *Tissue Eng.* **2007**, *13*, 2087–2094.
- (28) Nishi, Y.; et al. Establishment and characterization of a steroidogenic human granulosa-like tumor cell line, KGN, that expresses functional follicle-stimulating hormone receptor. *Endocrinology* **2001**, *142*, 437–445.
- (29) Ford, J. M.; Bruggemann, E. P.; Pastan, I.; Gottesman, M. M.; Hait, W. N. Cellular and biochemical characterization of thioxanthenes for reversal of multidrug resistance in human and murine cell lines. *Cancer Res.* **1990**, *50*, 1748–1756.
- (30) Robey, R. W.; Lin, B.; Qiu, J.; Chan, L. L. Y.; Bates, S. E. Rapid detection of ABC transporter interaction: Potential utility in pharmacology. *J. Pharmacol. Toxicol. Methods* **2011**, *63*, 217–222.
- (31) Hanna, E. A.; et al. Gap junctional intercellular communication and connexin-43 expression in human ovarian surface epithelial cells and ovarian carcinomas *in vivo* and *in vitro*. *Carcinogenesis* **1999**, *20*, 1369–1373.
- (32) Davidson, J. S.; Baumgarten, I. M.; Harley, E. H. Reversible inhibition of intercellular junctional communication by glycyrrhetic acid. *Biochem. Biophys. Res. Commun.* **1986**, *134*, 29–36.
- (33) Gregor, T.; Bialek, W.; de Ruyter van Steveninck, R. R.; Tank, D. W.; Wieschaus, E. F. Diffusion and scaling during early embryonic pattern formation. *Proc. Natl. Acad. Sci. U.S.A.* **2005**, *102*, 18403–18407.

- (34) Kirkpatrick, J. P.; Brizel, D. M.; Dewhirst, M. W. A mathematical model of tumor oxygen and glucose mass transport and metabolism with complex reaction kinetics. *Radiat. Res.* **2003**, *159*, 336–344.
- (35) Abbaci, M.; Barberi-Heyob, M.; Blondel, W.; Guillemin, F.; Didelon, J. Advantages and limitations of commonly used methods to assay the molecular permeability of gap junctional intercellular communication. *Biotechniques* **2008**, *45*, 33–61.
- (36) Bao, B.; Jiang, J.; Yanase, T.; Nishi, Y.; Morgan, J. R. Connexon-mediated Cell Adhesion Drives Microtissue Self-assembly. *FASEB J.* **2011**, *25*, 255–264.
- (37) Lee, K. S.; Tsien, R. W. Mechanism of calcium channel blockade by verapamil, D600, diltiazem and nitrendipine in single dialysed heart cells. *Nature* **1983**, *302*, 790–794.
- (38) Ferry, D. R.; Traunecker, H.; Kerr, D. J. Clinical trials of P-glycoprotein reversal in solid tumours. *Eur. J. Cancer* **1996**, *32A*, 1070–1081.
- (39) Tolcher, A. W.; et al. Phase I crossover study of paclitaxel with r-verapamil in patients with metastatic breast cancer. *J. Clin. Oncol.* **1996**, *14*, 1173–1184.
- (40) Bao, B.; Jiang, J.; Yanase, T.; Nishi, Y.; Morgan, J. R. Connexon-mediated cell adhesion drives microtissue self-assembly. *FASEB J.* **2011**, *25*, 255–264.
- (41) Chan, H. S.; et al. Combining cyclosporin with chemotherapy controls intraocular retinoblastoma without requiring radiation. *Clin. Cancer Res.* **1996**, *2*, 1499–1508.
- (42) Fracasso, P. M.; et al. Phase II study of paclitaxel and valsphodar (PSC 833) in refractory ovarian carcinoma: a gynecologic oncology group study. *J. Clin. Oncol.* **2001**, *19*, 2975–2982.
- (43) Desroches, B. R.; Zhang, P.; Choi, B.; Maldonado, A. E.; Rago, A.; Liu, G. X.; Nath, N.; King, M. E.; Hartmann, K. M.; Yang, B.; Koren, G.; Morgan, J. R.; Mende, U. Functional Scaffold-free Cardiac Microtissues: A Novel Model for the Investigation of Heart Cells. *Am. J. Physiol.* **2012**, *302*, H22031–H220442.
- (44) Achilli, T. M.; McCalla, S.; Tripathi, A.; Morgan, J. R. Quantification of the kinetics and extent of self-sorting in three dimensional spheroids. *Tissue Eng., Part C* **2012**, *18*, 302–309.